A Numerical Study of Turbulent Flame Speed Development in the Spherical Case

A. Lipatnikov and J. Chomiak

Department of Thermo- and Fluid Dynamics,
Chalmers University of Technology,
Gothenburg, 41296, Sweden
e-mail: lipatn@tfd.chalmers.se

Abstract

Physical mechanisms contributing to the increase in turbulent spherical flame speed as the kernel grows are numerically studied using the Turbulent Flame Speed Closure Model. Both the time-dependence of the mean reaction rate, invoked by the model, and the reduction of the curvature of the averaged kernel surface contribute to the increase at small flame radii. As the radius increases, the former effect relaxes and the latter dominates.

Introduction

Numerous experiments [1, 2, 3, 4, 5] with statistically spherical flame kernels expanding in a premixed turbulent gas have shown that the flame speed $S_t = d\bar{r}_f/dt$ increases as the flame radius $\bar{r}_f$ grows. The physical mechanisms governing this effect have not been clarified yet and different viewpoints can be found in the literature. The importance of flame-generated turbulence is stressed in Ref. [5]. Ashurst [6] highlights the transient behavior of the flow induced by the hot gas expansion. Bradley et al. [4] emphasize that as a kernel grows, it experiences a wider range of the turbulence spectrum and the burning velocity increases. The latter explanation appears to be most widely used.

The goal of the work is to asses the role played by various physical mechanisms contributing to the increase in the S_t of moderately large (comparable with the integral turbulence length scale L) flames under a slight pressure rise.

The model

Simulations of expanding flames were performed using the Turbulent Flame Speed Closure Model (TFSCM) put forward by Zimont (see Refs. [7] and [8] and the references therein). The model yields the following closed balance equation for the Favre averaged progress variable

$$\frac{\partial\bar{\rho}\tilde{c}}{\partial t} + \frac{\partial}{\partial x_j}(\bar{\rho}\tilde{u}_j\tilde{c}) = \frac{\partial}{\partial x_j}\left[\bar{\rho}(\kappa + D_t)\frac{\partial\tilde{c}}{\partial x_j}\right] + \frac{\bar{\rho}\,(1-\tilde{c})}{t_r(1+D_t/\kappa_b)}\exp\left(-\frac{\Theta}{T_u(1-\tilde{c}+\gamma\tilde{c})}\right) + \tag{1}$$
$$+ A\rho_u u'\left[\frac{L}{u'\tau_c}\right]^{1/4}\left\{1+\frac{\tau'}{t}\left[\exp\left(-\frac{t}{\tau'}\right)-1\right]\right\}^{1/2}\left\{\sum_{j=1}^{3}\left(\frac{\partial\tilde{c}}{\partial x_j}\right)^2\right\}^{1/2}$$

where the well-known time-dependent turbulent diffusivity approximation [9]

$$D_t = D_{t,\infty}\left[1 - \exp\left(-\frac{t}{\tau'}\right)\right], \tag{2}$$

is used. Here, t is the time counted beginning with ignition; x_j and u_j are the coordinates and flow velocity components, respectively; ρ is the gas density; $\tau_c = \kappa_u/S_L^2$ and $\tau' = D_{t,\infty}/u'^2$ are the chemical and turbulent time scales, respectively; $D_{t,\infty}$ is the steady turbulent diffusivity; u' is the r.m.s. turbulent velocity; $\gamma = \rho_u/\rho_b$ is the density ratio; κ is the heat diffusivity of the mixture; Θ is the activation temperature of a single global combustion reaction. The time scale t_r of this reaction is calculated so that it yields the known value of the laminar burning velocity S_L for the planar steadily propagating flame at $u' = 0$. The model includes a single constant $A = 0.4$ for various mixtures [8, 10].

The model has been validated [7, 8, 10] against an experimental data base obtained by 7 different teams for expanding, spherical, turbulent flames. For these purposes, unsteady balance equations for mass, mass fractions of the fuel and oxidant, and mixture enthalpy supplemented by the TFSCM, the ideal gas state equation, and the standard $k-\epsilon$ model of turbulence were numerically solved. The governing equations, boundary and initial conditions, input parameters, and other details are reported in Ref. [8]. Figure 1 shows that the model well predicts flame speed development. These and numerous other tests summarized in Ref. [10] support the use of the TFSCM for the objectives of the work.

The following mechanisms contributing to the development of turbulent spherical flame speed are addressed by the model. First, the last source term on the right-hand side (RHS) of Eq. 1 depends directly on time. The model of this time-dependence is discussed, in detail, elsewhere [8].

Second, the expansion of gases in the flame induces a flow and increases the flame speed as compared with the constant density case. For a flame of a steady structure and finite thickness, $\bar{\rho} = \bar{\varrho}(r - \bar{r}_f(t))$, the effect is controlled by the density ratio

$$< \gamma >^{-1} \equiv \frac{2}{\rho_u \bar{r}_f^2} \int_0^{\bar{r}_f} \bar{\varrho}(x - \bar{r}_f) x dx, \tag{3}$$

averaged over the en-flamed area. Indeed, the mass conservation equation has the following solution

$$\tilde{u} = \frac{d\bar{r}_f}{dt} \left[1 - \frac{2}{\bar{\rho} r^2} \int_0^r \bar{\varrho}(x - \bar{r}_f) x dx \right]. \tag{4}$$

Then, the flame speed with respect to the unburned mixture is equal to

$$S_{t,u} = S_t - \tilde{u}_{r=\bar{r}_f} = S_t \frac{2}{\bar{\rho}_{r=\bar{r}_f} \bar{r}_f^2} \int_0^{\bar{r}_f} \bar{\varrho}(x - \bar{r}_f) x dx = S_t < \gamma >^{-1} \tag{5}$$

if the flame radius $\bar{r}_f$ is associated with the leading edge of the flame and $\bar{\rho}_{r=\bar{r}_f} = \rho_u$.

Due to the finite thickness of the flame, $< \gamma >^{-1} > \gamma^{-1} = \rho_b / \rho_u$. As a result, the speed of the spherical flame, $< \gamma > S_{t,u}$, is slower than the speed of the planar flame, $\gamma S_{t,u}$, if the values of $S_{t,u}$ are the same. The effect is controlled by the ratio of the flame thickness to its radius. As the spherical kernel grows, the ratio decreases and $< \gamma >$ tends to γ. As a result, flame speed increases.

To illustrate the third mechanism, let us consider a simple balance equation modeling turbulent combustion in the planar ($a = 0$) and spherical ($a = 2$) cases

$$\bar{\rho} \frac{\partial \tilde{c}}{\partial t} + \bar{\rho} \left(\tilde{u} - a \frac{\kappa + D_t}{r} \right) \frac{\partial \tilde{c}}{\partial r} = \frac{\partial}{\partial r} \left[\bar{\rho} (\kappa + D_t) \frac{\partial \tilde{c}}{\partial r} \right] + \bar{W}. \tag{6}$$

In the latter case, the flame speed is slower due to the last term on the left-hand side of Eq. 6. The effect is controlled by the ratio of $(\kappa + D_t)/(\bar{r}_f S_t)$, characterizing the magnitude of the curvature term as compared with the convective one. This ratio decreases with time due to a more rapid flame radius growth as compared with $D_t \sim t^{1/2}$ [8]. As a result, the flame speed increases.

The second and third mechanisms are well known for laminar flames [11] where effects of them are of the order of $\delta_L / r_f \ll 1$, where $\delta_L = \kappa_u / S_L$ is the laminar flame thickness. In the turbulent case, the mean flame brush thickness δ_t is substantial and these mechanisms are much more pronounced.

To rank the above mechanisms, certain simulations (see short-dashed curve in Fig. 1 and symbols in Fig. 2) have been performed by decreasing D_t as [12]

$$D_t = D_{t,\infty} \left[1 - \exp\left(-\frac{t}{\tau'} \right) \right] \left[1 - \exp\left(-\frac{\bar{r}_f}{L} \right) \right]. \tag{7}$$

It is worth emphasizing that this work does not address the validity of Eq. 7 because, for these purposes, Eq. 1 should correspondingly be modified. Here, Eq. 7 is used as a method of analysis only in order to assess the role of diffusivity by decreasing it as compared to the basic case (Eq. 2).

Results and discussion

The results show that a smaller D_t (Eq. 7) corresponds to a higher flame speed and slower evolution of S_t (compare solid and short-dashed curves in Fig. 1). A smaller diffusivity is associated with a thinner flame brush (compare squares and dotted curve in Fig. 2) and a higher spatial maximum $\tilde{v}_m$ of the

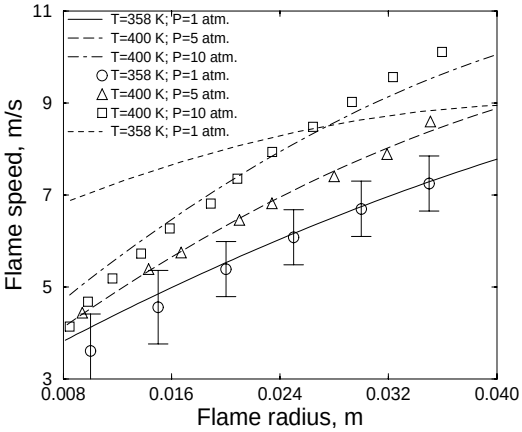

Figure 1: Flame speed vs. flame radius ($\tilde{c} = 0.1$). Symbols show the experimental data of Bradley et al. [4] with the vertical bars indicating the mean scatter of the data obtained for 9 equivalent runs. The short-dashed curve has been computed with Eq. 7 for $D_t(t, \bar{r}_f)$, other ones have been computed with Eq. 2 for $D_t(t)$. The stoichiometric iso-octane/air mixture, $u' = 2.36$ m/s, $L = 20$ mm, initial values of pressure P and temperature T are presented in the figure legends.

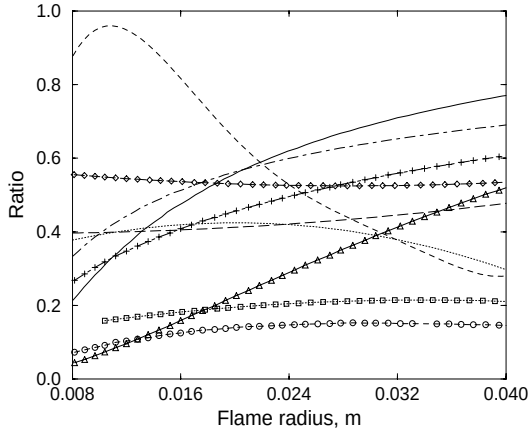

Figure 2: Evolution of various ratios computed either with Eq. 2 (curves) or with Eq. 7 (symbols). Solid curve and triangles show $D_t/D_{t,\infty}$ (see Eqs. 2 and 7); dotted-dashed curve and pluses correspond to the dimensionless sum of the two source terms on the RHS of Eq. 1; dotted curve and squares show $\delta_t/\bar{r}_f$; long-dashed curves and diamonds correspond to $\tilde{v}_m/S_t$; dashed curve and circles show $2D_t/(\tilde{v}_m\bar{r}_f)$. Initial conditions correspond to the solid curve in Fig. 1.

gas flow velocity (diamonds and long-dashed curve). However, this effect is too weak (diamonds and long-dashed curve are close enough) to explain the strong influence of the submodel of D_t, shown in Fig. 1. Moreover, when using Eq. 2, the ratio of $\tilde{v}_m/S_t$ increases too slowly to explain the transient behavior of S_t (compare the solid curve in Fig. 1 and long-dashed curve in Fig. 2). These results suggest that the second mechanism (see Eqs. 3-5) is of secondary importance. The dotted-dashed curve and pluses in Fig. 2 indicate that the source terms on the RHS of Eq. 1 evolves similarly in both cases.

The process of elimination suggests that the third, mean curvature mechanism can cause the difference between the solid and dashed curves in Fig. 1. When using Eq. 2, the ratio of $D_t/(\tilde{v}_m\bar{r}_f)$, characterizing the importance of the mechanism, is high for small flame radii and decreases with $\bar{r}_f$ (dashed curve in Fig. 2). Consequently, the mean curvature effect strongly reduces S_t when $\bar{r}_f$ is small but this effect relaxes as $\bar{r}_f$ increases. To the contrary, this ratio is small and roughly constant when computing D_t from Eq. 7 (circles). As a result, the flame speed is higher and increases slower.

To assess the role played by the first mechanism, the development of the source term on the RHS of Eq. 1 has been suppressed at various boundary flame radii r_b, i.e., t_b, associated with $\bar{r}_f(t_b) = r_b$, has been substituted in the last source term instead of t when $\bar{r}_f > r_b$ and $t > t_b$. The results are presented in Fig. 3. For small flame radii, this suppression strongly affects flame speed. The effect is markedly weaker for $r_b = 16$ mm and is of minor importance for $r_b \geq 24$ mm.

The above results show that the development of turbulent spherical flame speed is controlled by the mean curvature (the third) mechanism for moderately large flames. Since the same mechanism leads to the linear relation between the flame speed and δ_L/r_f in the laminar case [11], one may expect a linear relation between S_t and $\delta_t/\bar{r}_f$. The processed data computed for the turbulent spherical flames indicate a linear dependence (see Fig. 4). Following the methods elaborated for the laminar flames [11], such a process can be used to evaluate the fully developed turbulent flame speeds associated with the intersection between the ordinate axis and approximating straight lines. The obtained values agree well with the steady-limit values of S_t computed for the asymptotically stationary planar flames.

Conclusions

Physical mechanisms affecting the increase of turbulent spherical flame speed have been numerically studied. Both the time-dependence of the mean reaction rate and the mean curvature contribute to the increase at small flame radii. As the radius increases, the former effect relaxes and the latter dominates. A method for evaluating fully developed turbulent flame speeds has been proposed.

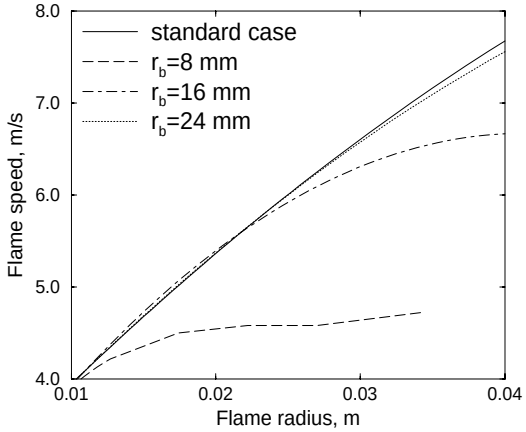

Figure 3: Flame speed vs. flame radius. The dashed, dotted-dashed, and dotted curves have been computed by suppressing the increase of the last source term on the RHS of Eq. 1 with time when $\bar{r}_f > r_b$. Initial conditions correspond to the solid curve in Fig. 1.

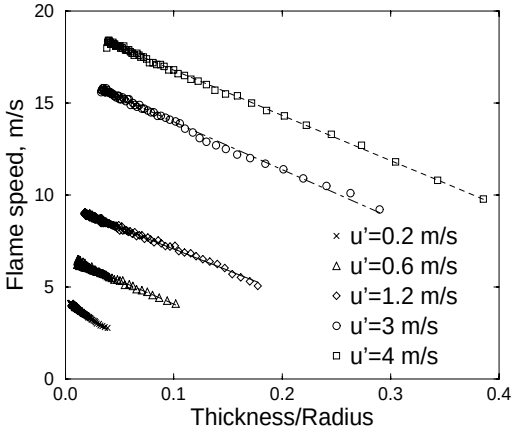

Figure 4: Turbulent flame speed S_t *vs* the ratio of the mean flame brush thickness δ_t to the flame radius $\bar{r}_f$. Symbols have been computed, curves linearly approximate the computed results. The stoichiometric iso-octane/air mixture, $T = 358$ K, $P = 1$ bar, $L = 8$ mm.

Acknowledgment

This work was supported by the Chalmers Combustion Engine Research Center.

References

[1] R. G. Abdel-Gayed, K. J. Al-Khishali, and D. Bradley. Turbulent Burning Velocities and Flame Straining in Explosions. *Proc. R. Soc. London*, A391:393–414, 1984.

[2] E. G. Groff. An Experimental Evaluation of an Entrainment Flame Propagation Model. *Combust. Flame*, 67:153–162, 1987.

[3] D. S.-K. Ting, M. D. Checkel, R. Haley, and P. R. Smy. Early Flame Acceleration Measurements in a Turbulent Spark-Ignited Mixture. *SAE Paper* 940687 (1994).

[4] D. Bradley, M. Lawes, and C. G.W. Sheppard. Study of Turbulence and Combustion Interaction: Measurement and Prediction of the Rate of Turbulent Burning. Report. Leeds University, 1995.

[5] B. Leisenheimer and W. Leuckel. Self-Generated Acceleration of Confined Deflagrative Flame Fronts. *Combust. Sci. Technol.*, 118:147–164, 1996.

[6] Wm. T. Ashurst. A Simple Illustration of Turbulent Flame Ball Growth. *Combust. Sci. Technol.*, 104:19–32, 1995.

[7] V. P. Karpov, A. N. Lipatnikov, and V. L. Zimont. A Test of an Engineering Model of Premixed Turbulent Combustion. *26th Symp. (Int.) on Combust.*, The Combustion Institute, Pittsburgh, pp.249–257, 1996.

[8] A. N. Lipatnikov and J. Chomiak. A Simple Model of Unsteady Turbulent Flame Propagation. *SAE Paper* 972993, 1997.

[9] J. O. Hinze. *Turbulence*, 2nd ed. McGraw-Hill, New York, 1975.

[10] A. Lipatnikov, J. Wallesten, and J. Nisbet. Testing of a Model for Multi-Dimensional Computations of Turbulent Combustion in Spark Ignition Engines. *COMODIA 98,* JSME, pp.239–244, 1998.

[11] Ya. B. Zel'dovich, G. I. Barenblatt, V. B. Librovich, and G. M. Makhviladze. *The Mathematical Theory of Combustion and Explosions.* Plenum Publ. Corp., New York, 1985.

[12] R. Herweg and R. R. Maly. A Fundamental Model for Flame Kernel Formation in S.I. Engines. *SAE Paper* 922243, 1992.